Title
Ohm’s law for ion conduction in lithium and beyond-lithium battery electrolytes

Journal
The Journal of Chemical Physics, 151(2)

ISSN
0021-9606

Authors
Galluzzo, Michael D
Maslyn, Jacqueline A
Shah, Deep B
et al.

Publication Date
2019-07-14

DOI
10.1063/1.5109684

Peer reviewed

Ohm's Law for Ion Conduction in Lithium and Beyond-Lithium Battery Electrolytes

Michael D. Galluzzo[†,1,2], Jacqueline A. Maslyn[†,1,2], Deep B. Shah[†,1,2,3], and Nitash P. Balsara[1,2,3]*

[1]Department of Chemical and Biomolecular Engineering University of California, Berkeley, CA 94720, United States.

[2]Materials Science Division, Lawrence Berkeley National Laboratory, Berkeley, CA 94720, United States

[3]Joint Center for Energy Storage Research (JCESR), Lawrence Berkeley National Laboratory, Berkeley, CA 94720, United States.

[†]These authors contributed equally to this work

AUTHOR INFORMATION

Corresponding Author

* Correspondence to: nbalsara@berkeley.edu

ABSTRACT

The viability of next generation lithium and beyond-lithium battery technologies hinges on the development of electrolytes with improved performance. Comparing electrolytes is not straightforward, as multiple electrochemical parameters affect the performance of an electrolyte. Additional complications arise due to the formation of concentration gradients in response to dc potentials. We propose a modified version of Ohm's law to analyze current through binary electrolytes driven by a small dc potential. We show that the proportionality constant in Ohm's law is given by the product of the ionic conductivity, κ, and the ratio of currents in the presence (i_{ss}) and absence (i_{Ω}) of concentration gradients, $\rho_{+¿¿}$. The importance of $\rho_{+¿¿}$ was recognized by J. Evans, C.A. Vincent, and P.G. Bruce [*Polymer* 28, 2324 (1987)]. The product $\kappa\rho_{+¿¿}$ is used to rank order a collection of electrolytes. Ideally, both κ and $\rho_{+¿¿}$ should be maximized, but we observe a trade-off between these two parameters, resulting in an upper bound. This trade-off is analogous to the famous Robeson upper bound for permeability and selectivity in gas separation membranes. Designing polymer electrolytes that overcome this trade-off is a worthwhile but ambitious goal.

MAIN TEXT

I. INTRODUCTION

In a battery, the passage of ionic current between the cathode and anode is enabled by the electrolyte. The dependence of the current on the potential drop between the electrodes is at the core of battery design and engineering.[1,2] The kind of device that can be powered by a battery is limited by the maximum current that can be passed safely through the electrolyte.

The starting point for understanding the relationship between potential drop and current is Ohm's law. For a simple conductor with one charge carrier, such as a copper wire (Fig. 1a), the current density, i, is proportional to the potential drop per unit length, $\Delta V/L$, and Ohm's law can be written as:

$$i = \sigma \frac{\Delta V}{L}, \tag{1}$$

where σ is the electronic conductivity of the material. All materials are electrically neutral and have at least two charge carriers; the one charge carrier approximation is valid because the compensating copper cations are essentially immobile. Current density versus $\Delta V/L$ for copper is presented in Fig. 1b, where the slope, m, is given by 5.8×10^5 S cm^{-1}.[3] In this case, $m = \sigma$. For a copper wire, carrier concentration gradients do not develop as the copper cations are stationary and charge neutrality is maintained.

1

2

(a)

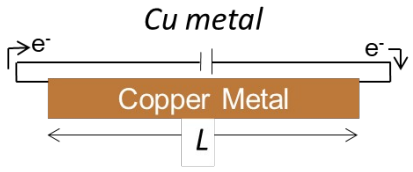
Cu metal
e-
e-
Copper Metal
L

(b)

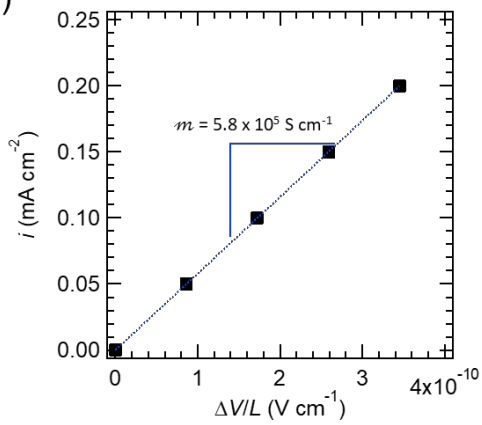
m = 5.8 x 10^5 S cm^-1
i (mA cm^-2)
ΔV/L (V cm^-1)
4x10^-10

(c)

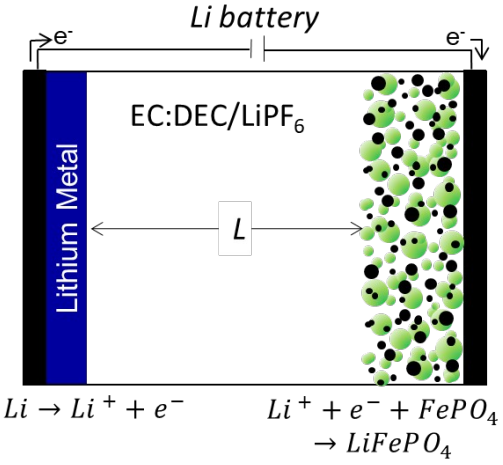
Li battery
e-
e-
EC:DEC/LiPF6
Lithium Metal
L
Li → Li+ + e−
Li+ + e− + FePO4 → LiFePO4

(d)

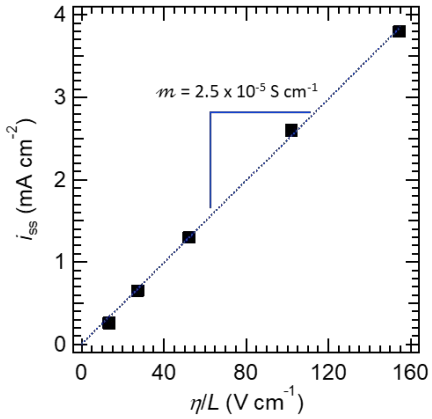
m = 2.5 x 10^-5 S cm^-1
iss (mA cm^-2)
η/L (V cm^-1)

(e)

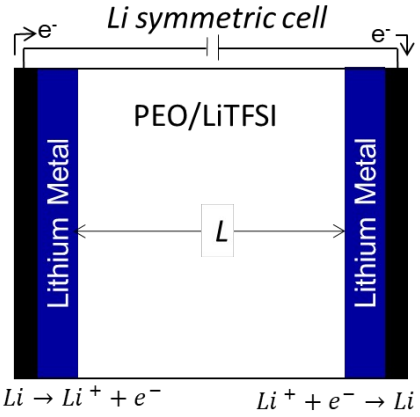
Li symmetric cell
e-
e-
PEO/LiTFSI
Lithium Metal
Lithium Metal
L
Li → Li+ + e−
Li+ + e− → Li

(f)

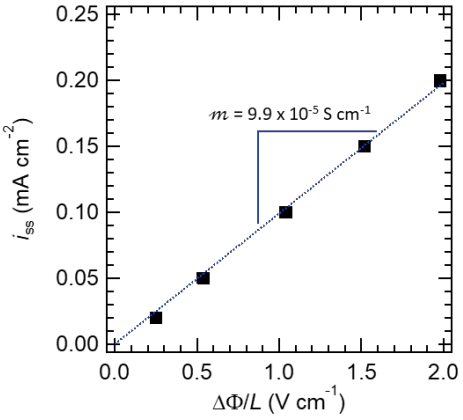
m = 9.9 x 10^-5 S cm^-1
iss (mA cm^-2)
ΔΦ/L (V cm^-1)

3

Figure 1. Empirical relationship between current density and normalized potential drop across three types of cells. a) Schematic of a piece of copper metal, which is an electronic conductor. b) Current density, i, as a function of normalized voltage drop, V/L, for the copper metal depicted in Fig 1a. Adapted from Ref.3. c) Schematic of a battery with a lithium metal anode, a lithium iron phosphate cathode, and an EC:DEC/$LiPF_6$ electrolyte. d) Steady-state current density, i_{ss}, as a function of normalized overpotential, ¿L, for the battery depicted in Fig. 1c. Adapted from Ref.4. e) Schematic of a lithium symmetric cell containing a PEO/LiTFSI electrolyte. f) Steady-state current density, i_{ss}, as a function of normalized voltage drop over the electrolyte, Φ/L, in the cell depicted in Fig. 1e. Adapted from Ref.5. The difference between values of m obtained in electronic and ionic conductors is ten orders of magnitude.

An example of a rechargeable battery is shown schematically in Fig. 1c. It consists of a lithium metal anode and a lithium iron phosphate, $LiFePO_4$, cathode separated by an EC:DEC/$LiPF_6$ electrolyte in a porous separator. During discharge, the passage of ionic current through the electrolyte from the anode to the cathode is driven by an overpotential, η, which is the equilibrium potential of the cell minus the operating voltage, $U^0 - V$.[1] When an overpotential is present, concentration gradients develop across the electrolyte because both cations (in this case, Li^+) and anions (PF_6^{-}¿¿) are mobile in the system. Under a constant overpotential, this would result in a time-dependent current density until the concentration gradient reaches steady-state. Only Li^+ ions are transported across electrode/electrolyte

interfaces; this also affects the nature of the gradients. In Fig. 1d, we plot the steady-state current density, i_{ss}, as a function of the overpotential per unit length, η/L, for the cell depicted in Fig. 1c.[4] It appears that the relationship between i_{ss} and η/L is approximately linear, similar to the copper wire. However, the slope, m = 2.5 $\times 10^{-5}$ S cm^{-1}, is not equal to the conductivity of the electrolyte. It reflects numerous processes that include charge transfer between the electrodes and the electrolyte, diffusion of lithium in the cathode, and diffusion and migration of ions in the electrolyte. Thus, the relationship between i_{ss} and η/L in Fig. 1d, although it appears linear, is not a manifestation of Ohm's law.–

In Fig. 1e, a schematic for a symmetric cell consisting of an electrolyte sandwiched between two identical non-blocking electrodes is presented. In this perspective, we focus on symmetric cells comprising either lithium or sodium foil electrodes and electrolytes containing a lithium or sodium salt, respectively. This cell, popularized by pioneering work of Evans, Vincent, and Bruce, and others,[6–8] is similar to that shown in Fig. 1c with one crucial difference: $U^0 = 0V$. This cell enables a fair comparison of the ion transport properties of different electrolytes: the symmetry of the cell allows electrode effects to be deconvoluted from the properties of the electrolyte. In Fig. 1f, we plot i_{ss} as a function of the potential drop across the electrolyte, $\Delta\Phi/L$, for a cell with lithium foil electrodes and an electrolyte comprising poly(ethylene oxide) (PEO) and bis(trifluoromethylsulfonyl)amine lithium salt (LiTFSI).[5]

Here, the slope $m = 9.9 \times 10^{-5}$ S cm^{-1} is not equal to the ionic conductivity of the electrolyte. However, unlike in a full battery, m is related to the properties of the electrolyte alone. In our effort to design high performance electrolytes, it is the slope in Fig. 1f which we wish to maximize. Many publications, however, disregard this. It is fairly common, these days, to invent a new electrolyte, measure the ionic conductivity, and declare victory if it is greater than that of a baseline electrolyte.

The purpose of this perspective is to analyze symmetric cell data obtained from different electrolytes. Evans, Bruce, and Vincent[6,9] and Watanabe et al.,[10] modeled symmetric cells containing dilute and ideal electrolytic solutions. In later studies, Newman and coworkers[1,11] considered symmetric cells containing concentrated electrolytic solutions and developed the relationships between m and intrinsic transport and thermodynamic properties of the electrolyte. This perspective is focused on small applied potentials wherein the concentration dependence of the relevant electrolyte properties can be neglected. Based on the work in Refs.5–11, we develop a framework for measuring the Ohm's law coefficient which allows us to produce a rank ordered list of electrolytes based on their ability to maximize the flux of lithium or sodium cations. We conclude by discussing the limitations of our approach as, ultimately, the rank ordering of electrolytes needs to be reassessed in the presence of significant concentration gradients for practical devices.

II. THEORY

Electrolytes of interest comprise a salt ¿¿¿dissolved in a matrix. Characterization of ion transport typically begins with measurement of the ionic conductivity, κ, by ac impedance spectroscopy. A powerful feature of ac impedance spectroscopy is that κ is measured without introducing significant concentration gradients. When a dc potential, $\Delta\Phi$, is applied across an electrolyte of dimension L in a symmetric cell (Fig. 1e), there are, by definition, no concentration gradients at the first instant of polarization ($t = 0^+$). The initial current density, i_0, at $t = 0^+$ is given by:

$$i_0 = \kappa \frac{\Delta\Phi}{L}. \quad (2)$$

With time, i.e. at $t > 0$, salt concentration gradients develop in the cell and eventually the gradient becomes time-invariant. The measured current density decreases with time as these concentration gradients develop and reaches a steady value at long times. We refer to the current obtained at long times as i_{ss}.

In the limit of small applied potentials, an expression for i_{ss} can be derived based on concentrated solution theory,[11,12]

$$i_{ss} = \frac{\kappa}{1+Ne} \frac{\Delta\Phi}{L}, \quad (3)$$

where Ne is a dimensionless parameter that we call the Newman number. Ne is given by

$Ne = a\kappa RT$ where R is the gas constant, T is the temperature, F is Faraday constant, D is the restricted diffusion coefficient of the salt, c is the salt concentration, t_{+}^{0} is the transference number of the cation with respect to the velocity of the solvent, $\gamma_{\pm}$ is the mean molal activity coefficient of the electrolyte, and m is the salt molality. The parameter a is related to the stoichiometry of the salt:

$$a = \frac{\nu}{\nu_{+} z_{+}}$$

where ν is the total number of cations and anions to which the salt dissociates, ν_{+} is the total number of cations to which the salt dissociates, and z_{+} is the charge number of the cation. (For a binary salt, $a = 2$.) Equations 3 and 4 are based on Newman's concentrated solution theory wherein electrolytes are characterized by three transport parameters, κ, D, and t_{+}^{0}, and a thermodynamic factor, $T_f = 1 + \frac{d \ln \gamma_{\pm}}{d \ln m}$. This theory builds on the work of Onsager[13] who recognized that ion transport in binary electrolytes is governed by three Stefan-Maxwell diffusion coefficients, D_{0-}, D_{0+}, and $D_{\pm}$. Relationships between κ, D, and t_{+}^{0}, and the Stefan-Maxwell diffusion coefficients are given in Ref.11.

While all four parameters (κ, D, t_{+}^{0}, and T_f) dictate the time-dependent current at a given applied potential, explicit knowledge of all

these parameters is not required to determine i_{ss} or Ne. In fact, Ne can be determined in a single experiment by measuring i_0 and i_{ss} at constant dc polarization, $\Delta\Phi$, over the electrolyte:

$$\frac{i_{ss}}{i_0} = \frac{1}{1+Ne}. \quad (6)$$

Bruce and Vincent pioneered the measurement of i_{ss}/i_0.[6,9]

Equations 6 and 4 can be recast as:

$$\frac{i_{ss}}{i_0} = \beta + \frac{t_{+¿^0}}{\beta+1}¿ \quad (7)$$

where

$$\beta = \nu_{-¿} \frac{D_{0+¿}}{D_{\pm¿} \frac{c}{c_0} ¿} \quad (8) ¿$$

and c_0 is the solvent concentration. Equations 7 and 8 were first derived by Balsara and Newman.[11] Only in the limit $c \to 0$, $\beta \to 0$ does

$$\frac{i_{ss}}{i_0} ¿ t_{+¿^0, ¿} \quad (9)$$

a result presented by Bruce and Vincent.[9] Determining the range of concentration over which β is small enough such that Eq. 9 is valid requires knowledge of the Stefan-Maxwell diffusion coefficients. For dilute 0.01 M aqueous potassium chloride (Fig. 14.1 of Ref.1), $D_{\pm¿¿}$= 1.1 x 10^{-7} cm^2 s^{-1}, $D_{0+¿¿}$

1= 1.9 x 10^{-5} cm^2 s^{-1}, c_0 = 56 mol L^{-1}, β = 0.031 and Eq. 9 is a good 2approximation. However, most practical electrolytes are not dilute. For a 1 M 3aqueous potassium chloride solution, $D_{\pm ¿¿}$= 1.9 x 10^{-6} cm^2 s^{-1}, $D_{0+¿¿}$= 2.0 x 10^{-} 4^5, c_0= 53.6 mol L^{-1}, and β= 0.20. For 2.6 M PEO/LiTFSI (Fig. 3 and 4 of 5Ref.14), $D_{\pm ¿¿}$= 4.0 x 10^{-9} cm^2 s^{-1}, $D_{0+¿¿}$ = 1.1 x 10^{-8} cm^2 s^{-1}, c_0 = 16 mol L^{-1}, and 6β = 0.44. Equation 9 is not a good approximation for either 1M KCl or 2.6 M 7PEO/LiTFSI.

8 We thus define the current ratio, $\rho_{+¿¿}$, which can be rewritten on the 9basis of Eq. 6 as

10$\rho_{+¿=\frac{i_{ss}}{i_0}=\frac{1}{1+Ne}.¿}$ (10) The current ratio is an intrinsic property of an electrolyte, 11irrespective of whether it is dilute or concentrated. The transference number, 12$t_{+¿^0¿}$, is defined as the fraction of current carried by the cation in a solution of 13uniform salt concentration and is only approximated by $\rho_{+¿¿}$ when β is small.

14For this reason, we prefer to use $\rho_{+¿¿}$ to refer to the current ratio, $\frac{i_{ss}}{i_0}$, rather 15than using $t_{+¿^0¿}$ or "the transference number" as is commonly done in the 16literature. This point was alluded to by Bruce and Gray in 1995, who referred 17to this current ratio as "the limiting current fraction".[15]

18 The discussion thus far ignores the resistance of the 19electrode/electrolyte interface. In practice, when a dc voltage, ΔV, is 20supplied to a symmetric cell, the potential drop across the electrolyte, $\Delta\Phi$,

will be reduced by an amount equal to the product of the interfacial resistance and the current. Assuming other sources of ohmic loss are negligible,

$$\Delta\Phi = \Delta V - iR_i A \qquad (11)$$

where R_i is the interfacial impedance that is readily measured by ac impedance spectroscopy, A is the electrochemically active surface area of the electrode, and i is the current density through the symmetric cell. We can combine Eq. 2, 3, 10 and 11 to obtain a useful expression

$$\rho_{+,0} = \frac{i_{ss}}{i_0}\frac{\left(\Delta V - i_0 R_{i,0} A\right)}{\left(\Delta V - i_{ss} R_{i,ss} A\right)} \qquad (12)$$

where i_{ss} and i_0 refer to steady-state and initial current density through a symmetric cell as in Eq. 11. The importance of corrections for interfacial resistance was recognized by Evans, Bruce and Vincent[6] and Watanabe et al.[10] We use the term $\rho_{+,0}$ in Eq. 12 to clarify that this current ratio is based on a measured value of i_0, which we discuss next.

In order to apply Eq. 10-12, the value of i_0 must be measured. A practical approach is to take the first data point measured after the potential is applied. However, this method is inherently problematic because the current is a strong function of time in the first instant of polarization. An example of such a measurement is shown in Fig. 2. A small potential, ΔV = 8.9 mV, was applied across a lithium symmetric cell (A = 0.079 cm^2 and L = 0.050 cm) containing a 35 kg mol^{-1} PEO/LiTFSI electrolyte with salt concentration r = 0.010, where r is defined as the molar ratio of lithium ions to ethylene oxide

moieties. A sampling rate of 1 ms^{-1} was used for the first few seconds. Figure 2 presents the current response over the entire time window (400 min) required to reach steady-state and the inset highlights the first 10 ms. Over the first 10 ms, the current is approximately constant with time. Thus, we have confidence that the current density we measure, i_0 = 0.051 mA cm^{-2}, truly captures the initial current.

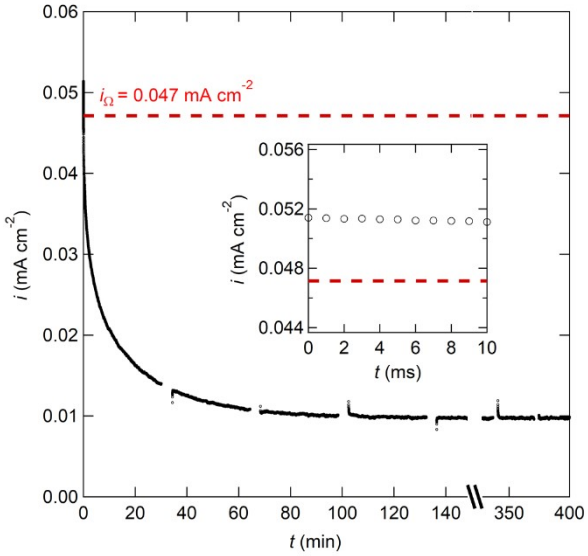

Figure 2. A plot of current density versus time in a lithium symmetric cell containing a PEO/LiTFSI electrolyte with r = 0.010 after applying a potential of ΔV =¿8.9 mV across the L = 0.050 cm electrolyte. The current response over the entire time window (400 min) required to reach a steady-state is presented as a function of time. (The breaks in the curve are due to ac impedance measurements.) The inset highlights the first 10 ms, when the current is approximately constant with time. The dashed red line represents the value of i_Ω= 0.047 mA cm^{-2} calculated from Eq. 14. The high sampling frequency at early times provides confidence that

the measured initial current density is accurate. In this case, the first measurement of current density (i_0=¿0.051 mA cm^{-2}) is in reasonable agreement with i_Ω.

An alternative that has been proposed[6,16–23] is to calculate i_0 by combining Eq. 2 and 11. In this case,

$$i_0 = \kappa \frac{(\Delta V - i_0 R_i A)}{L}. \quad (13)$$

We can rearrange Eq. 13 to solve for i_0. We refer to this calculated current density as i_Ω because it is a statement of Ohm's law (Eq. 1):

$$i_\Omega = \frac{\Delta V}{L/\kappa + R_i A}. \quad (14)$$

For the electrolyte and cell used in Fig. 2, κ = 0.33 mS cm^{-1} and R_i = 495 Ω, yielding i_Ω = 0.047 mA cm^{-2} (shown as a red dashed line in Fig. 2). We see reasonable agreement between i_0 and i_Ω from this experiment. The advantage of using i_Ω instead of i_0 is that it is based on parameters that are easily measured (ΔV, L, R_i, κ, and A). Further rationale for this is discussed in Section IV. For the purposes of this paper, we define $\rho_{+¿¿}$ as:

$$\rho_{+¿} = \frac{i_{ss}}{i_\Omega} \frac{(\Delta V - i_\Omega R_{i,0} A)}{(\Delta V - i_{ss} R_{i,ss} A)}.¿ \quad (15)$$

Eq. 15 differs from Eq. 12 only in the use of i_Ω for i_0. In the discussion below, electrolytes are characterized by two transport properties, κ and $\rho_{+¿¿}$. We use Eq. 15 to calculate $\rho_{+¿¿}$.

III. DATA

To select the systems used in this perspective, we studied the 472 papers which cited Evans, Vincent, and Bruce's 1987 paper titled "Electrochemical measurement of transference numbers in polymer electrolytes"[6] since 2010. Only a small fraction of these papers reported all parameters necessary for our analysis. These parameters are listed in Table I.

Table I. List of parameters related to the Evans, Vincent, and Bruce measurement of i_{ss}/i_0 gathered for the electrolyte systems described in this study. We also list their symbols and descriptions.

Parameter	Symbol	Description
ionic conductivity, blocking	κ_b	ionic conductivity of the electrolyte measured by ac impedance using blocking electrodes (e.g. stainless steel)
ionic conductivity, non-blocking	κ_{nb}	ionic conductivity measured by ac impedance using non-blocking electrodes (e.g. lithium metal)
applied voltage	ΔV	constant voltage applied by the potentiostat in order to elicit a steady-state current density
current density, initial	i_0	initial current density measured after polarization at ΔV
current density, steady-state	i_{ss}	current density measured at steady-state in response to ΔV
interfacial resistance, initial	$R_{i,0}$	interfacial resistance measured by ac impedance spectroscopy just before ΔV is applied

interfacial resistance, steady-state	$R_{i,ss}$	interfacial resistance measured by ac impedance spectroscopy after the steady-state current is reached
bulk resistance	R_b	bulk resistance measured in the cell during the steady-state current experiment
cell thickness	L	distance between electrodes; electrolyte thickness
interfacial area	A	nominal electrode area in contact with the electrolyte

1

2 The four categories of electrolytes covered in this study are pictured in
3Fig. 3: homopolymer electrolytes containing a lithium salt and no solvent
4(HPE), gel polymer electrolytes containing a crosslinked polymer mixed with
5a solvent and a lithium salt (GPE), polymer electrolytes containing a sodium
6salt (NaPE), and multicomponent polymer electrolytes containing a polymer
7mixed with a salt and at least one additional component (MCPE). The
8additional component in the MCPEs may be another polymer (blended or
9covalently bonded), an ionic liquid, or a ceramic particle. All of the
10electrolytes were designed to transport lithium ions except for those placed
11in the sodium electrolyte category. A long-form description of each
12electrolyte, its category, and its reference is provided in Table II.

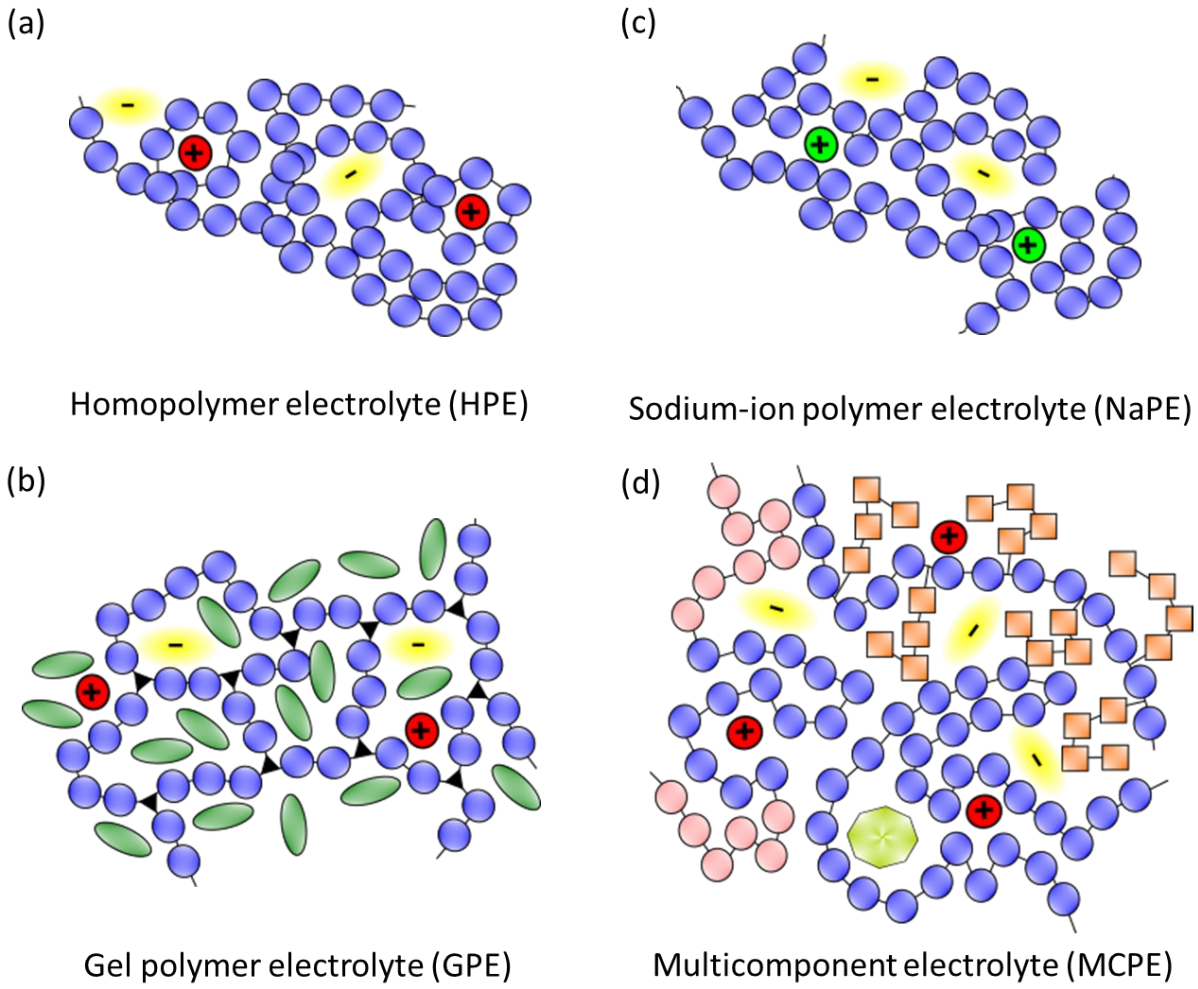

Figure 3. Schematics of the four categories of electrolytes analyzed in this perspective. (a) Simple homopolymer electrolytes containing a lithium salt (HPE). Blue spheres represent monomer beads on a polymer chain, red spheres indicate lithium cations, and yellow ovals represent the negative counterion. (b) Gel or crosslinked polymer electrolytes (GPE). Black triangles represent crosslinks in a polymer network and green ovals represent solvent molecules. (c) Polymer electrolytes containing a sodium salt (NaPE). Green spheres represent sodium cations. (d) Multicomponent polymer electrolytes (MCPE). The schematic depicts several types of MCPEs. Pink spheres represent a second monomer type on a copolymer chain, orange cubes represent ionic liquid side chains grafted to a

1polymer chain, and the green octagon represents a nanoparticle dispersed in the 2polymer.

3

4**Table II.** Long-form descriptions of the electrolyte systems analyzed in this 5perspective and their categories: HPE – homopolymer electrolyte, GPE – gel polymer 6electrolyte, MCPE – multicomponent polymer electrolyte, NaPE – sodium ion polymer 7electrolyte.

Electrolyte description	Category	Ref
polyethylene oxide with bis(trifluoromethylsulfonyl)amine lithium salt (PEO/LiTFSI) with 0.017 moles of LiTFSI per mole of ether oxygen (r = 0.017)	HPE	21
PEO/LiTFSI with r = 0.08	HPE	17
poly(diethylene oxid-alt-oxymethylene) with LiTFSI (P(2EO-MO)/LiTFSI) with 0.04 moles of LiTFSI per mole of oxygen (r = 0.04)	HPE	18
P(2EO-MO)/LiTFSI with r = 0.08	HPE	18
P(2EO-MO)/LiTFSI with r = 0.14	HPE	18
perfluoroether containing 8 carbon atoms with dimethyl carbonate end groups and bis(fluorosulfonyl)imide lithium salt (C8-DMC/LiFSI) with 5.84 wt% LiFSI	HPE	22
C8-DMC/LiFSI with 19.9 wt% LiFSI	HPE	22
perfluoropolyether with hydroxyl end groups containing 10 fluoro-ether oxygens ($PFPE_{D10}$-Diol) and 9.1 wt% LiTFSI	HPE	23
perfluoropolyether with dimethyl carbonate end groups containing 10 fluoro-ether oxygens ($PFPE_{D10}$-DMC) and 9.1 wt% LiTFSI	HPE	23
PEO/LiTFSI gel mixed with tetraethylene glycol dimethyl ether (TEGDME)	GPE	24
80 wt% methoxy-PEO-methacrylate and 20 wt% hexadecal-PEO-methacrylate copolymerized into a matrix (PMH20) with $LiClO_4$ salt	GPE	25
crosslinked PEO plasticized by TEGDME with LiTFSI	GPE	26
PEO/LiTFSI blended with poly[(trifluoromethyl)sulfonyl acrylamide] (PA-LiTFSI)	MCPE	27

$Li_7La_3Zr_2O_{12}$ (LLZO) dispersed in poly(vinylidene fluoride-hexa-fluoropropylene) (PVDF-HFP)	MCPE	28
polyhedral oligomeric silsesquioxane (POSS) grafted with ionic liquid (IL) side chains doped with LiTFSI	MCPE	29
perfluoropolyether with 2 ethylene oxide units on each end terminated with dimethyl carbonate end groups containing 10 fluoro-ether oxygens ($PFPE_{E10}$-DMC) and 9.1 wt% LiTFSI	MCPE	23
corn starch crosslinked with γ-(2,3-Epoxypropoxy)propyltrimethoxy-silane with LiTFSI	MCPE	30
PEO blended with sodium carboxyl methyl cellulose (Na-CMC) with sodium perchlorate ($NaClO_4$)	NaPE	31
organic ionic plastic crystals consisting of triisobutylmethylphosphonium bis(fluorosulfonyl)imide with added bis(fluorosulfonyl)imide sodium salt (NaFSI)	NaPE	32

For each electrolyte in Table II, we calculated $\rho_{+¿¿}$ using Eq. 15 and the values of the parameters we obtained from the publication. For some references, all parameters were listed explicitly. In others, we needed to estimate the parameters from raw data such as Nyquist impedance spectra or current versus time plots. In three cases, the parameters needed were supplied in a personal communication from the authors.[17,18,32] Finally, if our calculated value for $\rho_{+,0}$ differed substantially from the reported value (usually referred to by others as $t_{+¿¿}$), the reference was not included in this study. Only 13 out of the 472 papers satisfied all of the constraints. The most common reason a paper was excluded from our analysis was not reporting L and A. Unfortunately, we could not find any papers which characterized single ion conductors that met all our requirements.

IV. CHARACTERIZATION OF ELECTROLYTE PERFORMANCE

In most papers, the reported current ratio is based on the measured value of i_0. One criterion for including papers in this study was that all parameters needed to calculate i_Ω from Eq. 14 were reported. We were thus able to calculate $\rho_{+¿¿}$ using Eq. 15 and compare it with the reported value, $\rho_{+,0}$, obtained using Eq. 12. Fig. 4 is a plot of $\rho_{+¿¿}$ versus $\rho_{+,0}$ for the 19 electrolytes listed in Table 2. For references that report only $\rho_{+¿¿}$, we plot $\rho_{+¿=\rho_{+,0}¿}$: these are represented by filled in symbols. Points which lie on the dashed line in Fig. 4 indicate that the measured value of i_0 was consistent with the calculated value of i_Ω. A significant number of data points in Fig. 4 fall well below the dashed line. A likely reason for this is the use of a sampling rate that is too slow to capture i_0 accurately. Because the current density falls rapidly at early times (see Fig. 2), use of a less frequent sampling rate will result in a lower value of i_0 and thus an inflated value of $\rho_{+,0}$.

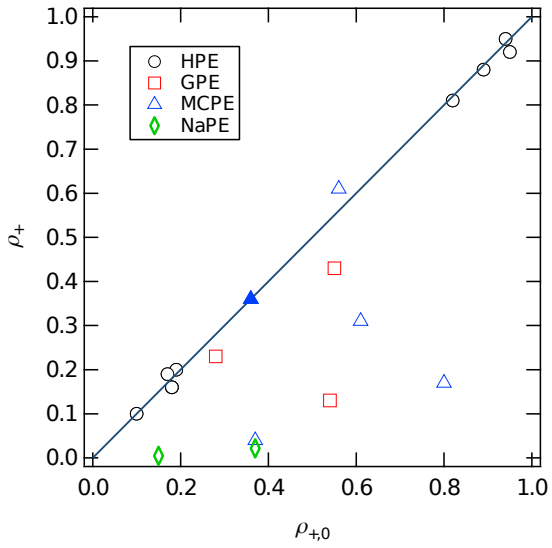

Figure 4. Comparison of $\rho_{+¿¿}$ calculated using different values for the initial current for the electrolytes in Table II. On the vertical axis, $\rho_{+¿¿}$ is calculated using the initial current from Ohm's law, i_Ω, as defined in Eq. 15. On the horizontal axis, $\rho_{+,0}$ is calculated using the measured initial current density, i_0, as defined in Eq. 12. The dashed line indicates the case where $i_\Omega = i_0$. For references that report only $\rho_{+¿¿}$, we plot $\rho_{+¿=\rho_{+,0}¿}$: these are represented by filled in symbols.

While using i_Ω to calculate $\rho_{+¿¿}$ has been proposed by some[6,16–23], the literature is dominated by reports of $\rho_{+,0}$ based on measured values of i_0. Our analysis suggests that $\rho_{+¿¿}$ is a more robust method for determining the current ratio of an electrolyte. For consistency, all calculations will utilize i_Ω beyond this point.

In principle, the conductivity of an electrolyte measured by ac impedance spectroscopy is a material property that should not depend on the electrodes used in the experiment. Either non-blocking electrodes (lithium or sodium

metal), or blocking electrodes (stainless steel, aluminum, etc.) can be used when conducting ac impedance spectroscopy. Conductivities measured using non-blocking or blocking electrodes are denoted κ_{nb} and κ_b, respectively. Fig. 5 presents κ_{nb} versus κ_b for the electrolytes in Table II. For many electrolytes, κ_{nb} is significantly lower than κ_b. A few electrolytes show the opposite trend. It is not immediately clear whether κ_{nb} or κ_b should be used to quantify the performance of an electrolyte. To answer this question, we rearrange Eq. 3 and 10 to obtain:

$$\kappa\rho_{+¿=\frac{i_{ss}}{\Delta\Phi/L}.¿} \quad (16)$$

This is a statement of Ohm's law for an electrolyte at steady-state under small polarization, where $\kappa\rho_{+¿¿}$ can be defined as the effective conductivity of the electrolyte at steady-state. In Fig. 6a we plot $\kappa_b\rho_{+¿¿}$ versus $\frac{i_{ss}}{\Delta\Phi/L}$, while in Fig. 6b we plot $\kappa_{nb}\rho_{+¿¿}$ versus $\frac{i_{ss}}{\Delta\Phi/L}$. The data in Fig. 6b are consistent with Eq. 16 while the data in Fig. 6a are not. Fig. 6 shows that only κ_{nb} can be used to accurately describe the experimental steady-state current. This is because $\rho_{+¿¿}$ and κ_{nb} are both measured in symmetric cells with non-blocking electrodes. For consistency, as we compare the $\rho_{+¿¿}$ of electrolytes, we must also use κ_{nb} when evaluating the performance of an electrolyte. Future studies aimed at characterizing new electrolytes should report both κ_b and

κ_{nb}. For cases where κ_b and κ_{nb} differ substantially, attempts should be made to understand the root cause as it may be an indication of electrolyte degradation or inconsistencies in cell fabrication. For ether-based polymer electrolytes, it may be an indication of physical dissolution (i.e. non-electrochemical) of lithium or sodium metal from the electrodes.[33]

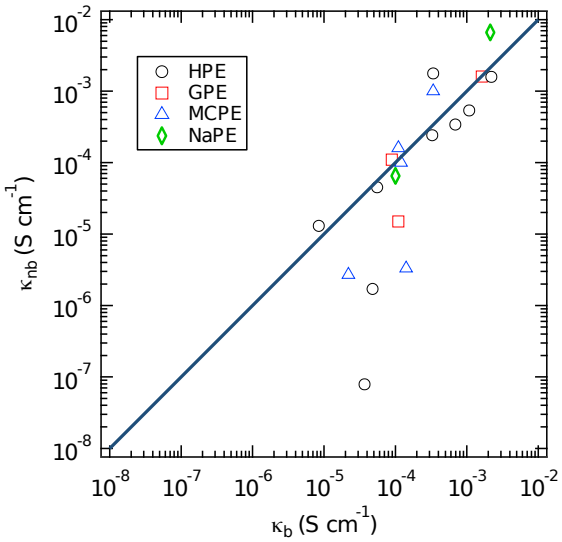

Figure 5. Ionic conductivity measured with non-blocking electrodes, κ_{nb}, versus ionic conductivity measured with blocking electrodes, κ_b. The dashed line represents the case where $\kappa_b = \kappa_{nb}$: principally, these two values should be the same.

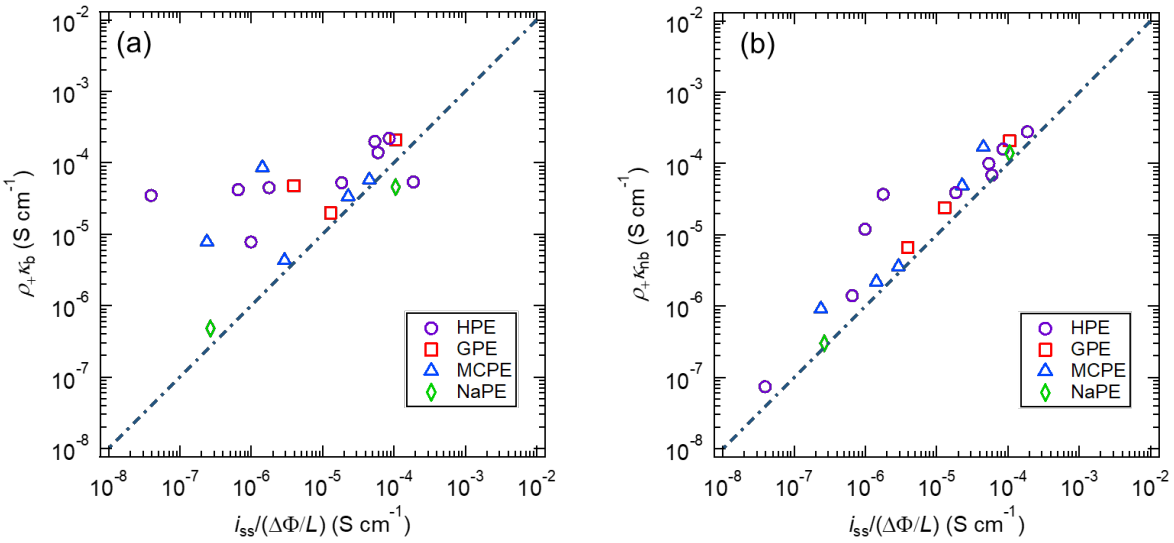

Figure 6. The effective conductivity, $\kappa\rho_{+¿¿}$, versus the measured steady-state current normalized by the voltage drop per unit length, $\frac{i_{ss}}{\Delta\Phi/L}$. (a) Plot with $\kappa=\kappa_b$, the conductivity measured with blocking electrodes and (b) Plot with $\kappa=\kappa_{nb}$, the conductivity measured with non-blocking electrodes. The dashed line represents Eq. 6, a statement of Ohm's law for electrolytes under dc polarization at steady-state. Only $\kappa_{nb}\rho_{+¿¿}$ data are reasonably consistent with Ohm's law. Rank ordering of electrolytes is thus based on $\kappa_{nb}\rho_{+¿¿}$.

V. TRADE-OFF BETWEEN CONDUCTIVITY AND SELECTIVE CATION TRANSPORT

In an electrolyte, both cations and anions are mobile, but our main interest is to maximize the flux of the working cation. This is similar to a gas separation process wherein a membrane is used to concentrate a desired species.[34,35] In this process, a pressure gradient is used to drive transport

through the membrane, which is designed such that one species is more permeable. Selective transport in this system is characterized by two parameters: (1) the permeability of species *i*, P_i, relates the molar flux and driving force ($\Delta P/L$¿, where ΔP is the pressure drop across a membrane of thickness L, and (2) the selectivity of species *i*, α_{ij}, which is defined as P_i/P_j where *j* refers to the other species being transported. Ideally, one would like to maximize both P_i and α_{ij}. The difficulty of realizing this ideal was noted by Robeson, who showed that membranes with high permeability typically had low selectivity while membranes with high selectivity had low permeability.[36] When data from a large number of membranes were compiled on a plot of selectivity versus permeability, a clear upper bound was evident. Robeson presented a straight line on a log-log plot of selectivity versus permeability such that all compiled data lay below this line. This is referred to as the Robeson upper bound for gas separation.

We present a similar analysis for ion transport in polymer electrolytes under a small dc potential. Selective transport in this system is characterized by two parameters: (1) the conductivity, κ, relates the total current, with contributions from both ions, and driving force ($\Delta\Phi/L$¿, and (2) the current ratio, $\rho_{+¿¿}$, which is a measure of selectivity for cation transport. Ideally, one would like to maximize κ and $\rho_{+¿.¿}$[37–39] In Fig. 7, we plot $\rho_{+¿¿}$ versus κ_{nb} for the electrolytes in Table II. The line in Fig. 7 is analogous to the Robeson upper

bound. The upper bound is defined empirically by $\rho_{+¿=-0.64-0.34\log\kappa_{nb}¿}$, where κ_{nb} is in S cm^{-1} and $\rho_{+¿¿}$ is bounded between 0 and 1.

The best electrolyte would be one that supports the highest steady-state current density for a given applied potential, i.e. maximizing the slope in Fig. 1f, $m = \kappa_{nb}\rho_{+¿¿}$. Since both parameters have been calculated, we can rank order the electrolytes of interest. This is done in Table III, where the third column gives the product $\kappa_{nb}\rho_{+¿¿}$. For completeness, we also give values of κ_b, κ_{nb}, Ne, $\rho_{+¿¿}$, and $t_{+¿^0¿}$ (when known). The top six electrolytes are identified by their rank in Fig. 7. Interestingly, $\rho_{+¿¿}$ is less than or equal to 0.2 for all six. In other words, the best electrolytes to date rely on high ionic conductivity rather than selective transport of cations, and efforts to achieve a value of $\rho_{+¿¿}$ closer to 1 have come at the cost of a disproportionate reduction in ionic conductivity. Considerable research has focused on surpassing the Robeson upper bound because there is no physical reason that a membrane cannot surpass it. The same is true for polymer electrolytes: future research aimed at surpassing the upper bound presented in Fig. 7 seems warranted.

While our analysis focuses on the bulk properties of the electrolyte, we recognize the importance of the electrolyte/electrode interface. Both interfacial resistance and the stability of the electrolyte/electrode interface contribute to the efficacy of an electrolyte in a battery. Our approach accounts for interfacial resistance (Eq. 11-15). The rank ordering of electrolytes is, however, based on bulk properties alone.

1**Table III.** Rank ordered list of electrolytes included in this study, in order of largest 2to smallest $\kappa_{nb}\rho_{+¿¿}$. The top-ranked electrolyte is the most efficacious. Rank, 3electrolyte description, effective conductivity at steady-state ($\kappa_{nb}\rho_{+¿¿}$), blocking 4electrode conductivity (κ_b), non-blocking electrode conductivity (κ_{nb}), Newman 5number (Ne), current ratio ($\rho_{+¿¿}$), transference number $t_{+¿^0¿}$ (when known), category, 6and reference are presented for each electrolyte. All calculated parameters are 7taken from the reference by methods described in Section III.

Rank	**Electrolyte (Ref)**	$\kappa_{nb}\rho_{+¿¿}$ **[mS/cm]**	κ_b **[mS/cm]**	κ_{nb} **[mS/cm]**	*Ne*	$\rho_{+¿¿}$	$t_{+¿^0¿}$	**Category**
1	PEO/LiTFSI with r = 0.017 [21]	0.28	0.34	1.8	5.4	0.16		HPE
2	PEO/LiTFSI gel mixed with TEGDME [24]	0.21	1.6	1.6	6.8	0.13		GPE
3	Crosslinked cornstarch with LiTFSI [30]	0.17	0.34	1.0	4.9	0.17		MCPE
4	PEO/LiTFSI with r = 0.08 [17]	0.16	2.2	1.58	9.07	0.10	0.43	HPE
5	Organic ionic plastic crystals with NaFSI [32]	0.14	2.1	6.6	45	2.2×10^{-2}		NaPE
6	P(2EO-MO)/LiTFSI with r = 0.08 [18]	0.10	1.1	0.54	4.3	0.19		HPE
7	P(2EO-MO)/LiTFSI with r = 0.04 [18]	6.9×10^{-2}	0.69	0.34	3.9	0.20		HPE
8	LLZO dispersed in PVDF-HFP [28]	4.9×10^{-2}	0.11	0.16	2.3	0.31		MCPE
9	P(2EO-MO)/LiTFSI with r = 0.14 [18]	3.9×10^{-2}	0.33	0.24	5.2	0.16		HPE
10	C8-DMC with 19.9 wt% LiFSI [22,40]	3.7×10^{-2}	5.5×10^{-2}	4.5×10^{-2}	0.23	0.81	-0.07	HPE
11	PMH20/$LiClO_4$ [25]	2.4×10^{-2}	8.9×10^{-2}	0.11	3.4	0.23		GPE
12	C8-DMC with 5.84 wt% LiFSI [22,40]	1.2×10^{-2}	8.5×10^{-3}	1.3×10^{-2}	9.0×10^{-2}	0.92	-0.97	HPE
13	Crosslinked PEO/LiTFSI with TEGDME [26]	6.7E-03	0.110	1.5×10^{-2}	1.3	0.43		GPE
14	POSS with IL side chains and	3.6×10	0.120	0.10	27	$4.0\times10^{-}$		MCPE

	LiTFSI [29]	-3				2		
15	PEO/LiTFSI blended with PA-LiTFSI [27]	2.2×10 -3	0.141	3.3×1 0-3	0.64	0.61		MCPE
16	PFPED10-DMC with 9.1 wt% LiTFSI [23]	1.4×10 -3	4.8×10- 2	1.7×1 0-3	0.14	0.88		MCPE
17	PFPEE10-DMC with 9.1 wt% LiTFSI [23]	9.1×10 -4	2.2×10- 2	2.7×1 0-3	1.8	0.36		MCPE
18	PEO/Na-CMC blend with $NaClO_4$ [31]	3.0×10 -4	0.10	6.5×1 0-2	210	4.8×10- 3		NaPE
19	PFPED10-Diol with 9.1 wt% LiTFSI [23]	7.4×10 -5	3.70×1 0-2	7.9×1 0-5	5.0×1 0-2	0.95		MCPE

1

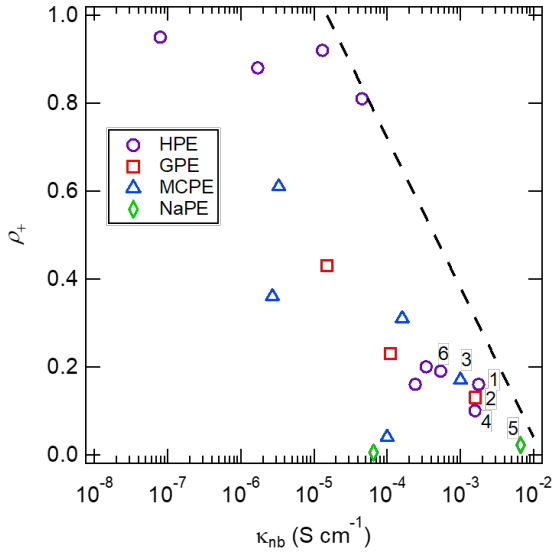

2

3 **Figure 7.** Plot of $\rho_{+¿¿}$ versus κ_{nb} for the electrolytes in Table II. The dashed line

4is analogous to the Robeson upper bound in gas separation membranes, here

5defined by $\rho_{+¿=-0.64-0.34\log\kappa_{nb}¿}$, where κ_{nb} is in S cm^{-1} and $\rho_{+¿¿}$ is bounded between 0

6and 1. The six electrolytes with the highest $\kappa_{nb}\rho_{+¿¿}$ in Table III are identified by their

7rank.

8 VI. DISCUSSION

The relationship between $\rho_{+¿¿}$ and transport properties of concentrated electrolytes is quantified by Eq. 4-7. In Table III, there are some electrolytes for which Ne is small (i.e., Ne ≤ 0.1), and others for which Ne is large (i.e., $Ne \geq 10$). In the limit of small Ne, $\frac{1}{1+Ne} \approx 1-Ne$ and Eq. 3 reduces to

$$i_{ss} = \kappa(1-Ne)\frac{\Delta\Phi}{L}, \quad (17)$$

which implies that the effective conductivity of the electrolyte at steady-state is marginally reduced from that at $t=0^{+¿¿}$ by a factor equal to $(1-Ne)$. When Ne is large, $1+Ne \approx Ne$ and Eq. 3 can be combined with Eq. 4 and written as

$$i_{ss} = \frac{F^2 Dc}{aRT¿¿¿}$$

The surprising conclusion from Eq. 18 is that there is a class of ion conductors for which the relationship between i_{ss} and $\Delta\Phi/L$ is independent of conductivity.

Maximizing $\rho_{+¿¿}$ is equivalent to minimizing Ne. It is clear from Eq. 4 that Ne may be reduced by either reducing κ, reducing $(1-t_{+¿^0¿})^2$, reducing T_f, or increasing D. Ultimately, we desire small values of Ne and large values of κ: thus, reducing Ne by reducing κ is not desirable. On the other hand, reducing $(1-t_{+¿^0¿})^2$, reducing T_f, or increasing D are desirable routes to increasing $\rho_{+¿¿}$.

There are very few publications where $t_{+¿^0¿}$, T_f, and D are measured.[2,14,16,40-41] Table III presents values of $t_{+¿^0¿}$ in cases where it has been reported. Note that there is little correspondence between $\rho_{+¿¿}$ and $t_{+¿^0¿}$.[17]

Our discussion has been limited to electrolytes under small applied dc potentials. Whether polarizations are large or small, the salt concentration gradients in the cell affect the current-voltage relationship. At large potential gradients obtained in practical batteries (Fig. 1c,d), the concentration dependence of κ, D, $t_{+¿^0¿}$, and T_f, can no longer be ignored, and rank ordering electrolytes would require numerical calculations described in Refs. 5,38.

VII. CONCLUSION

Ion transport through a binary battery electrolyte is governed by four concentration dependent parameters: κ, D, $t_{+¿^0¿}$, and T_f. Under large applied potentials typical of many battery applications, explicit knowledge of these four parameters and their concentration dependence is required to predict the relationship between i and $\Delta\Phi/L$. The problem is simplified for small applied potentials wherein two parameters govern the relationship between i and $\Delta\Phi/L$: κ and $\rho_{+¿¿}$. Data obtained from symmetric cells with non-blocking electrodes can be used to determine $\rho_{+¿¿}$ using Eq. 14 and 15. In principle, κ can be determined using either blocking (κ_b¿ or non-blocking electrodes (κ_{nb}¿ . Our study of the literature revealed a surprising discrepancy between these two measurements reported in a significant number of publications (see

Table III). When a discrepancy was found, κ_{nb} was often significantly lower than κ_b, although a few electrolytes show the opposite trend. While the analysis reported here is based on κ_{nb}, it is likely that practical electrolytes are those wherein the two conductivities are within experimental error, i.e., those that are unaffected by contact with the alkali metal of interest. Our analysis is restricted to publications wherein both κ_{nb} and $\rho_{+¿¿}$ were rigorously measured. Ideally, both κ_{nb} and $\rho_{+¿¿}$ should be maximized. However, there appears to be a trade-off between these two parameters, resulting in an upper bound ($\rho_{+¿=-0.64-0.34\log\kappa_{nb}¿}$, where κ_{nb} is in S cm^{-1}) that is analogous to one exposed by Robeson for the relationship between permeability and selectivity in gas separation membranes. Designing polymer electrolytes to surpass this upper bound may enable next-generation lithium and sodium batteries. In the limit of small applied potentials, the proportionality factor between i and $\Delta\Phi/L$ for binary electrolytes at steady-state is the product $\kappa_{nb}\rho_{+¿¿}$. This relationship is analogous to Ohm's law for electronic conductors. When comparing electrolyte performance, the preferred electrolyte is the one for which $\kappa_{nb}\rho_{+¿¿}$ is maximized. We use this principle to rank order electrolytes. We hope this perspective will serve as a guide for quantifying the efficacy of future electrolyte designs.

ACKNOWLEDGEMENT

This work was supported by the Joint Center for Energy Storage Research (JCESR), an Energy Innovation Hub funded by the U.S. Department of Energy (DOE), Office of Science, Basic Energy Sciences (BES), under Contract No. DEAC02-06CH11357. JAM was supported by a National Science Foundation Graduate Research Fellowship (DGE 2752814). We are grateful to Dr. Danielle Pesko for supplying portions of the data used in this perspective.

REFERENCES

1. J. Newman and K. Thomas-Alyea, *Electrochemical Systems III edition*, John Wiley &
Sons: Hoboken, NJ (2004).

2. Y. Ma, M. Doyle, T.F. Fuller, M.M. Doeff, L.C. De Jonghe, and J. Newman, J. Electrochem. Soc. **142**, 1859 (1995).

3. R.A. Matula, J. Phys. Chem. Ref. Data **8**, 1147 (1979).

4. V. Srinivasan and J. Newman, J. Electrochem. Soc. **151**, A1517 (2004).

5. D.M. Pesko, Z. Feng, S. Sawhney, J. Newman, V. Srinivasan, and N.P. Balsara, J. Electrochem. Soc. **165**, A3186 (2018).

6. J. Evans, C.A. Vincent, and P.G. Bruce, Polymer **28**, 2324 (1987).

7. P.R. Sørensen and T. Jacobsen, Electrochim. Acta **27**, 1671 (1982).

8. J.R. Macdonald, J. Chem. Phys. **58**, 4982 (1973).

19. P.G. Bruce and C.A. Vincent, J. Electroanal. Chem. **225**, 1 (1987).

210. M. Watanabe, S. Nagano, K. Sanui, and N. Ogata, Solid State Ion. **28–30**, 3911 (1988).

411. N.P. Balsara and J. Newman, J. Electrochem. Soc. **162**, A2720 (2015).

512. M. Doyle and J. Newman, J. Electrochem. Soc. **142**, 3465 (1995).

613. L. Onsager, Ann. N. Y. Acad. Sci. **46**, 241 (1945).

714. I. Villaluenga, D.M. Pesko, K. Timachova, Z. Feng, J. Newman, V. 8Srinivasan, and N.P. Balsara, J. Electrochem. Soc. **165**, A2766 (2018).

915. P.G. Bruce and F.M. Gray, in *Solid State Electrochem.*, edited by P.G. 10Bruce (Cambridge University Press, 1995), pp. 157–158.

1116. S. Zugmann, D. Moosbauer, M. Amereller, C. Schreiner, F. Wudy, R. 12Schmitz, R. Schmitz, P. Isken, C. Dippel, R. Müller, M. Kunze, A. Lex-Balducci, 13M. Winter, and J. Gores, J. Power Sources **196**, 1417 (2010).

1417. D.M. Pesko, K. Timachova, R. Bhattacharya, M.C. Smith, I. Villaluenga, J. 15Newman, and N.P. Balsara, J. Electrochem. Soc. **164**, E3569 (2017).

1618. Q. Zheng, D.M. Pesko, B.M. Savoie, K. Timachova, A.L. Hasan, M.C. Smith, 17T.F. Miller, W. Coates, and N.P. Balsara, J. Electrochem. Soc. **165**, A3186 18(2018).

1919. X. Li, W.S. Loo, X. Jiang, X. Wang, M.D. Galluzzo, K.I. Mongcopa, A.A. 20Wang, N.P. Balsara, and B.A. Garetz, Macromolecules. **52**, 982 (2019).

120. K.M. Abraham, Z. Jiang, and B. Carroll, Chem. Mater. **9**, 1978 (1997).

221. M.M. Hiller, M. Joost, H.J. Gores, S. Passerini, and H. Wiemhöfer,
3Electrochim. Acta **114**, 21 (2013).

422. D.B. Shah, K.R. Olson, A. Karny, S.J. Mecham, J.M. DeSimone, and N.P.
5Balsara, J. Electrochem. Soc. **164**, A3511 (2017).

623. M. Chintapalli, K. Timachova, K.R. Olson, S.J. Mecham, D. Devaux, J.M.
7Desimone, and N.P. Balsara, Macromolecules **49**, 3508 (2016).

824. H. Wang, M. Matsui, Y. Takeda, O. Yamamoto, D. Im, D. Lee, and N.
9Imanishi, Membranes **3**, 298 (2013).

1025. F. Cai, X. Zuo, X. M. Liu, L. Wang, W. Zhai, and H. Yang, Electrochim. Acta
11**106**, 209 (2013).

1226. L. Porcarelli, C. Gerbaldi, F. Bella, and J.R. Nair, Sci. Rep. **6**, 19892 (2016).

1327. M. Piszcz, O. Garcia-Calvo, U. Oteo, J.M. Lopez del Amo, C. Li, L.M.
14Rodriguez-Martinez, H.B. Youcef, N. Lago, J. Thielen, and M. Armand,
15Electrochim. Acta **255**, 48 (2017).

1628. W. Zhang, J. Nie, F. Li, Z.L. Wang, and C. Sun, Nano Energy **45**, 413
17(2018).

1829. G. Yang, H. Oh, C. Chanthad, and Q. Wang, Chem Mater. **29**, 9275
19(2017).

130. Y. Lin, J. Li, K. Liu, Y. Liu, J. Liu, and X. Wang, Green Chem. **18**, 3796 2(2016).

331. F. Colò, F. Bella, J.R. Nair, M. Destro, and C. Gerbaldi, Electrochim. Acta 4**174**, 185 (2015).

532. F. Makhlooghiazad, R. Yunis, D. Mecerreyes, M. Armand, P.C. Howlett, 6and M. Forsyth, Solid State Ion. **312**, 44 (2017).

733. M.D. Galluzzo, D.M. Halat, W.S. Loo, S.A. Mullin, J.A. Reimer, and N.P. 8Balsara, ACS Energy Lett. **4**, 903 (2019).

934. M. Mulder, *Basic Principles of Membrane Technology II edition*, Kluwer 10Academic: Dordrecht (1996).

1135. Y. Yampolskii and B. Freeman, *Membrane Gas Separation*, John Wiley &

12Sons: Hoboken, NJ (2010).

1336. L.M. Robeson, J. Memb. Sci. **62**, 165 (1991).

1437. M. Doyle, T.F. Fuller, and J. Newman, J. Electrochem. Soc. **140**, 1526 15(1993).

1638. M. Doyle, T.F. Fuller, and J. Newman, Electrochim. Acta **39**, 2073 (1994).

1739. K.M. Diederichsen, E.J. McShane, and B.D. McCloskey, ACS Energy Lett. **2**, 182563 (2017).

1940. D.B. Shah, H.Q. Nguyen, L.S. Grundy, K.R. Olson, S.J. Mecham, J.M. 20DeSimone, and N.P. Balsara, Phys. Chem. Chem. Phys. **21**, 7857 (2019).

141. L.O. Valøen and J.N. Reimers, J. Electrochem. Soc. **152**, A882 (2005).

242. H. Lundgren, M. Behm, and G. Lindbergh, J. Electrochem. Soc. **162**, 413

3(2015).

4

5LIST OF SYMBOLS

Symbol	Meaning
A	electrode area (cm^2)
a	salt stoichiometric coefficient
c	salt concentration (mol cm^{-3})
c_0	solvent concentration (mol cm^{-3})
D	restricted diffusion coefficient of the salt (cm^2 s^{-1})
$D_{0+¿¿}$	Stefan-Maxwell diffusion coefficient describing the interactions between the solvent and cation (cm^2 s^{-1})
$D_{0-¿¿}$	Stefan-Maxwell diffusion coefficient describing the interactions between the solvent and anion (cm^2 s^{-1})
$D_{\pm¿¿}$	Stefan-Maxwell diffusion coefficient describing the interactions between the cation and anion (cm^2 s^{-1})
F	Faraday constant (96485 C mol^{-1})
i	current density (mA cm^{-2})
i_0	initial current density measured after polarization at ΔV (mA cm^{-2})
i_{ss}	current density measured at steady-state in response to ΔV (mA cm^{-2})
i_Ω	initial current density calculated using Ohm's law at $t = 0^+$, see equation 14 (mA cm^{-2})
L	electrolyte or membrane thickness (cm)
m	slope
m	salt molality (mol kg^{-1})
M	general cation
Ne	Newman number
P_i	permeability of species i (mol m^{-1} s^{-1} Pa^{-1})
R	universal gas constant (8.314 J mol^{-1} K^{-1})
r	molar ratio of lithium cations to oxygens in the electrolyte
R_b	bulk resistance of the electrolyte measured by ac impedance spectroscopy (Ω)
R_i	interfacial resistance between electrolyte and non-blocking electrode (Ω)
$R_{i,0}$	interfacial resistance measured by ac impedance spectroscopy just before ΔV is applied (Ω)
$R_{i,ss}$	interfacial resistance measured by ac impedance spectroscopy after the steady-state current is reached (Ω)

T	temperature (K)
T_f	thermodynamic factor
t	time (s)
$t_{+¿^0¿}$	transference number of the cation with respect to the velocity of the solvent
U^0	battery open circuit potential (V)
V	battery operating voltage (V)
X	general anion
$z_{+¿¿}$	charge number of cation
$z_{-¿¿}$	charge number of anion

1
2
3GREEK
4

Symbol	Meaning
$\alpha_{i,j}$	selectivity of species i compared to species j
β	dimensionless parameter defined by Eq. 8
$\gamma_{\pm❑}$	mean molal activity coefficient of the electrolyte
$\Delta\Phi$	dc potential drop across an electrolyte, excluding ohmic drop across interfaces (V)
ΔP	pressure drop across a membrane (Pa)
ΔV	dc potential drop across a symmetric cell (V)
η	overpotential (V)
κ	ionic conductivity (S cm^{-1})
κ_b	ionic conductivity measured using blocking electrodes (S cm^{-1})
κ_{nb}	ionic conductivity measured using non-blocking electrodes (S cm^{-1})
ν	total number of ions to which the salt dissociates
$\nu_{+¿¿}$	number of cations in the dissociated salt
$\nu_{-¿¿}$	number of anions in the dissociated salt
$\rho_{+¿¿}$	current ratio obtained using i_Ω
$\rho_{+,0}$	current ration obtained using i_0
σ	electronic conductivity (S cm^{-1})

5